Behavior of Shape Memory Cu-Zn-Al Alloy Plates for Use in Energy Dissipators

P. Heresi, R. Herrera, M. O. Moroni
Universidad de Chile, Santiago, Chile

SUMMARY:
Shape Memory Alloys (SMA) are materials that can dissipate energy through hysteresis cycles without significant residual deformation. This paper describes the fabrication and testing of copper-based SMA hourglass-shaped plates for use in a dissipation device. The plates were tested under cyclic flexural deformations with increasing amplitudes at 0.2 Hz. The nominal composition of the SMA is Cu – 16.9%wt.Zn – 7.71%wt.Al – 0.04%wt.B. Proper thermo-mechanical treatments were applied in order to fabricate the plates. Also, cyclic tests of material coupons under tension loading were performed to obtain the stress-strain constitutive relationship of the material, applying deformations increasing linearly from 0 to 4%. The experimental data was then used to validate and calibrate a detailed non linear analytical model, based on previously conducted research.

Keywords: Shape memory alloy, Seismic dissipation devices, Experimental work.

1. INTRODUCTION

Shape Memory Alloys (SMA) are a class of materials that can dissipate energy through hysteresis cycles without significant residual deformation. SMA may present two types of phenomena, depending on the initial phase of the alloy (temperature and stress related). Both are the result of reversible phase transformation between Austenite and Martensite. Four temperatures define the phase transformation limits: start martensite (M_S), finish martensite (M_f), start austenite (A_s), and finish austenite (A_f). If the initial phase is Austenite, the alloy may present the Superelastic Effect (SE), which exhibits a hysteretic cycle, recovering its original shape after removal of the load. On the other hand, if Martensite is the initial phase, the alloy shows the Shape Memory Effect (SME), where the hysteretic cycle ends with residual deformation that can be recovered after heating. These self-centering and dissipating characteristics make SMAs a good material for seismic protection.

Nitinol, made of Ni and Ti has been used extensively in medicine and aeronautics. The use of this alloy in a wide range of seismic applications has also been investigated: Nitinol devices have been included as braces in steel frames (Asgarian et al. 2011), as connectors in beam-column joint of steel frames (Speicher et al. 2010) or as reinforcement in beam-column joints of reinforced concrete frames (Youssef et al. 2007). Recently, the inclusion of SMA devices in bridges has been reported by various authors (Johnson et al. 2008, Dong et al. 2011).

Copper based alloys have also shown shape memory capacity, but commercial fabrication has been restricted to small diameter wires and bars, where the most available alloy is CuAlBe. Research on copper based alloys has been mainly focused on the characterization of mechanic and thermal properties. This research has found that thermal treatment, grain size and sample size are key parameters that determine the SMA behaviour (Montecinos et al. 2008, Casciati et al. 2008).

Various analytical models have been developed to capture the constitutive law of SMA materials. Motahari and Ghassemieh (2007) proposed a multilinear curve to represent the stress-strain relation, which simulates various complex behaviors of SMAs, such as superelastic effect, partial superelastic effect, detwinning, and high rate loading (adiabatic conditions). This model stands out because of its simplicity and versatility.

This paper reports the findings of research on copper-based SMA hourglass-shaped plates for use in a dissipation device. These plates are fabricated and tested under cyclic flexure deformations with different amplitudes. Also, tests of material coupons under tension loading are performed to obtain the stress-strain constitutive relationship of the material. The experimental data is then used to validate and calibrate a detailed non-linear analytical model. Finally, a computational model of a complete SMA-based damper, suitable for use in large structural models, is developed and validated with experimental data.

2. EXPERIMENTAL STUDY

2.1 Samples preparation

Two CuZnAl alloys were prepared with nominal composition Cu - 16.90%wt.Zn - 7.71%wt.Al – 0.04%wt.B. Alloy A and alloy B were analyzed using optical spectroscopy, which yielded compositions of Cu - 17.43%wt.Zn - 7.48%wt.Al and Cu - 15.40%wt.Zn - 6.37%wt.Al, respectively. Each cast was forged to obtain a total of 8 rectangular plates of dimensions 150 mm x 300 mm x 15 mm.

A thermo-mechanical treatment was applied to all the plates. It consisted in heating the plate to 850ºC, pressing it to reduce its thickness and finally water quenching the plate. Each plate was machined to obtain a final thickness between 8 and 10.6 mm and an hourglass-shape, as shown in Fig. 2.1a. From each plate a coupon (Fig. 2.1b) to test in tension was also obtained. Differential Scanning Calorimeter (DSC) analysis and optical metallographies were performed to samples of the plates to establish the phase transformation temperatures M_s, M_f, A_s and A_f, to measure average grain sizes and to verify the initial phase. Martensite phase was observed at room temperature in all the samples. Average grain size was around 0.5 [mm]. Transformation temperatures of each alloy are shown in Table 1.

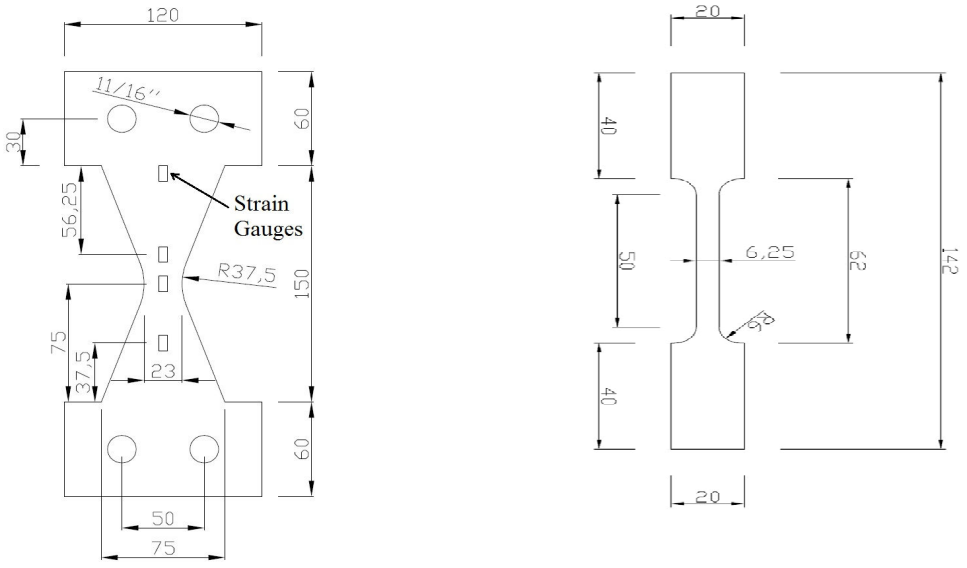

a) Plate dimension b) Coupon dimension

Figure 2.1. Samples Dimension in mm

Table 1. Phase Transformation Temperatures

Alloy	M_f [ºC]	M_s [ºC]	A_s [ºC]	A_f [ºC]
A	275	350	280	393
B	278	331	258	384

2.2 Experimental procedure and results

Flexural and tension tests were performed at the Georgia Institute of Technology using a MTS 810 Universal Testing Machine, equipped with MTS 647 Hydraulic Wedge Grips. A 250 kN load cell measured the force, while the grip displacement was measured by an internal LVDT. The actuator was set to run on displacement control for all the tests. In order to induce bending on the plates, a steel frame was designed and built. All the tests were performed at room temperature.

Material coupons were tested under cyclic tensile stresses at 0.025 and 1 Hz. Data was acquired at a sampling rate of 200 samples per second. For coupons P-1, P-4, P-5 and P-6, the deformation pattern consisted of 1 cycle at 0.5% followed by cycles of increasing amplitude at increments of 1% up to fracture. For coupons P-3, P-7 and P-8, the pattern was the same, but with amplitude increments of 0.5%. The coupon elongation was estimated from the grip displacement, considering that the compliance of the testing machine accounted for less than 0.1% of this value. Fig. 2.2 shows the stress-strain curves obtained for both alloys at the two different frequencies. The envelope curve is nearly bilinear, with transformation stresses about 190 MPa and 265 MPa and transformation strains of 0.6% and 0.9% for alloy A and B, respectively. The shape of the curves is characteristic of martensite and it is similar to that obtained by Gibson (2008), although, transformation limits of both alloys are higher in this study. Residual deformations in every cycle are noticeable. No frequency dependence is observed in the stress-strain behavior, and alloy B has a larger ductility than alloy A. On coupons P-7 and P-8, deformation pattern was stopped at 3.5% strain without fracture, to allow for further thermal analyses.

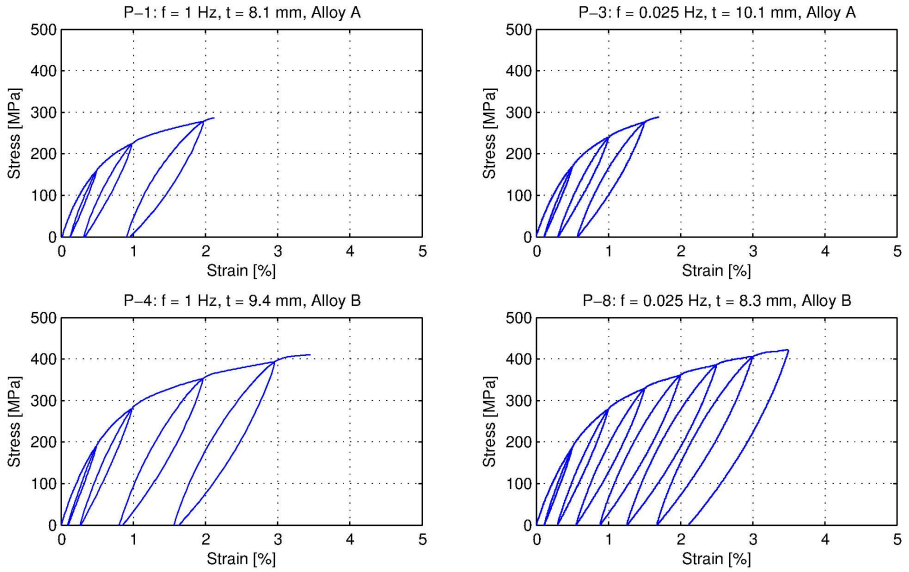

Figure 2.2. Stress-strain relationships from tensile coupon test

Cyclic sine deformations at increasing amplitudes and a constant frequency of 0.2 [Hz] were imposed to the plates. The deformation pattern applied to each specimen is shown in Fig. 2.3. Instrumentation consisted on the internal measurement of force and displacement, and 8 strain gauges on each plate as shown in Fig 2.1a. The location of the strain gauges was determined to capture the distribution of curvature and axial deformation along the height of the plate. Data was recorded at 100 samples per second.

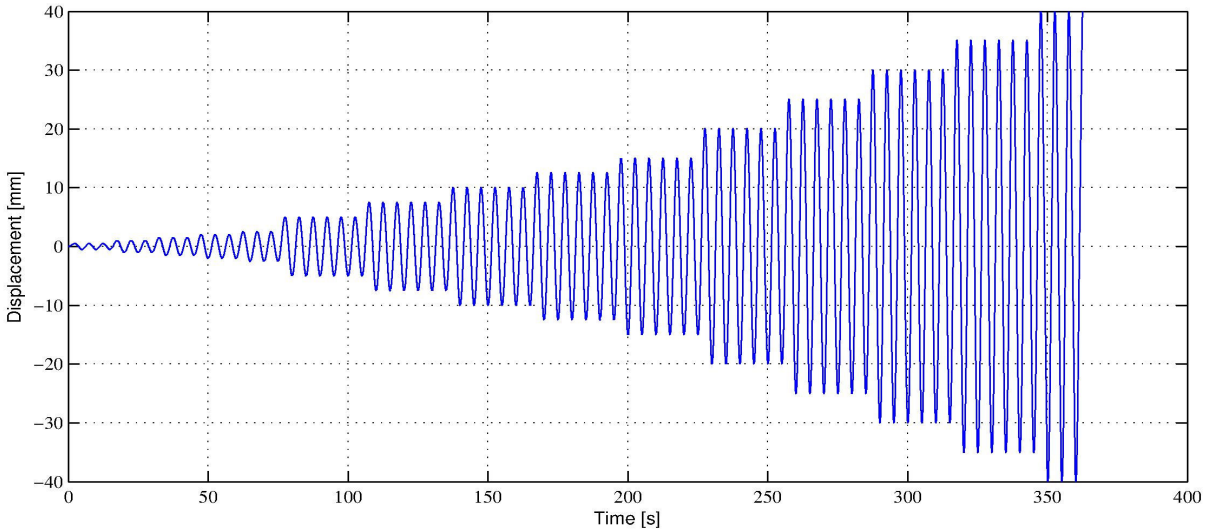

Figure 2.3. Displacement pattern for plate tests.

Fig. 2.4 shows overall force-displacement curves obtained for one representative specimen of each alloy. These results are similar in shape to those obtained by Vargas (2007). As expected from tensile tests, the alloy B withstood larger displacements before fracture occurred. The behavior of the plates is stable and symmetric while dissipating energy with no strength degradation. Fig. 2.5a and b show the distribution of axial strain, obtained from strain gauge measurements, on the upper and lower fibers. With this data, curvature and total axial deformation were computed (Fig. 2.5c and d). As expected, for low drift values ($\gamma = d/h$, with d: maximum displacement imposed and h: height of the plate), curvature is nearly constant along the height and total axial deformation is negligible. For higher drift values, the curvature significantly increases at the ends, while some axial deformations are perceptible, indicating the development of membrane action. Strains are shown up to 13.4% drift (displacement amplitude of 20 [mm]) since for larger values the strain gauges failed (gauge maximum strain was 2%).

For all plates, Effective Stiffness (K_{sec}), Energy loss (E_d) and Equivalent Viscous Damping Ratio (β_{eq}) were computed for each cycle (see Eqn. 2.1. and Eqn 2.2).

$$K_{sec} = \frac{|F^+| + |F^-|}{|d^+| + |d^-|} \tag{2.1}$$

$$\beta_{eq} = \frac{E_d}{4\pi \cdot E_s} \tag{2.2}$$

Where $|F^+|$, $|F^-|$, $|d^+|$ and $|d^-|$ are the maximum and minimum force and displacement of the cycle. The energy loss (E_d) corresponds to the total area of the hysteresis cycle, while E_s is the maximum elastic energy of the cycle.

Cycles with the same amplitude were averaged, obtaining these results as a function of the displacement amplitude imposed.

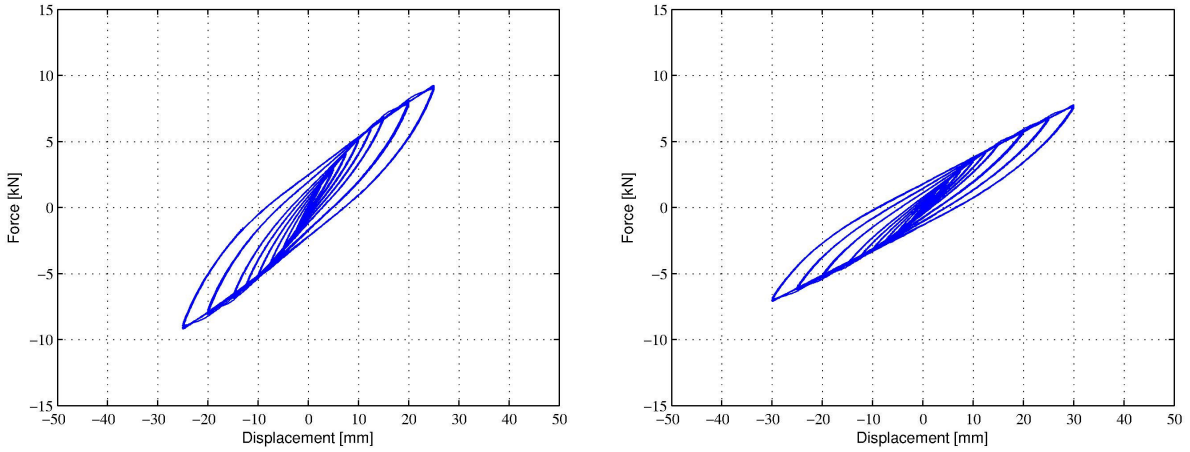

a) plate-3: Alloy A b) plate-5: Alloy B

Figure 2.4. Overall Force-Displacement curve.

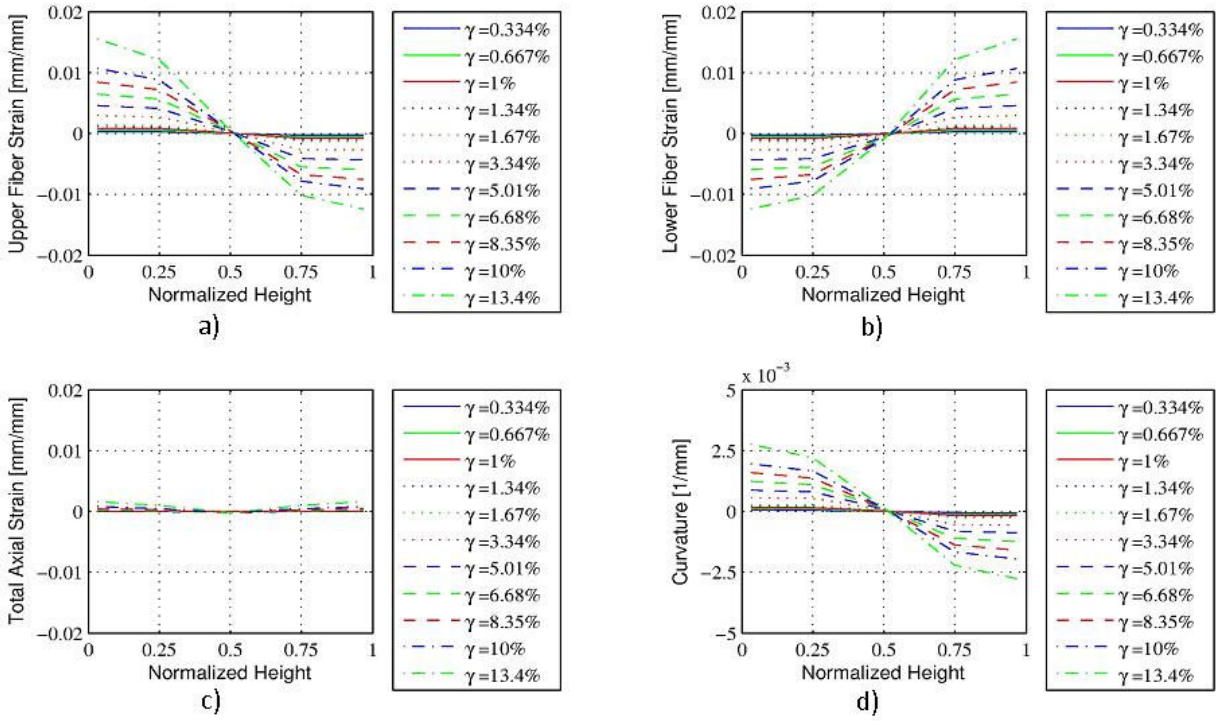

Figure 2.5. Strain and Curvature recorded across the plate height. Plate-3, Alloy A.

Fig. 2.6 shows the variation of the average effective stiffness, normalized by the initial stiffness, with drift. The effective stiffness diminishes significantly with the displacement: for 16.6% drift the effective stiffness decreases to 50% of the initial value. The average Energy loss per volume is shown in Fig. 2.7a. Energy loss increases for larger drift. The equivalent damping ratio is shown in Fig. 2.7b. It can be seen that it increases with the displacement imposed, reaching values up to 13% for the larger drift cycles.

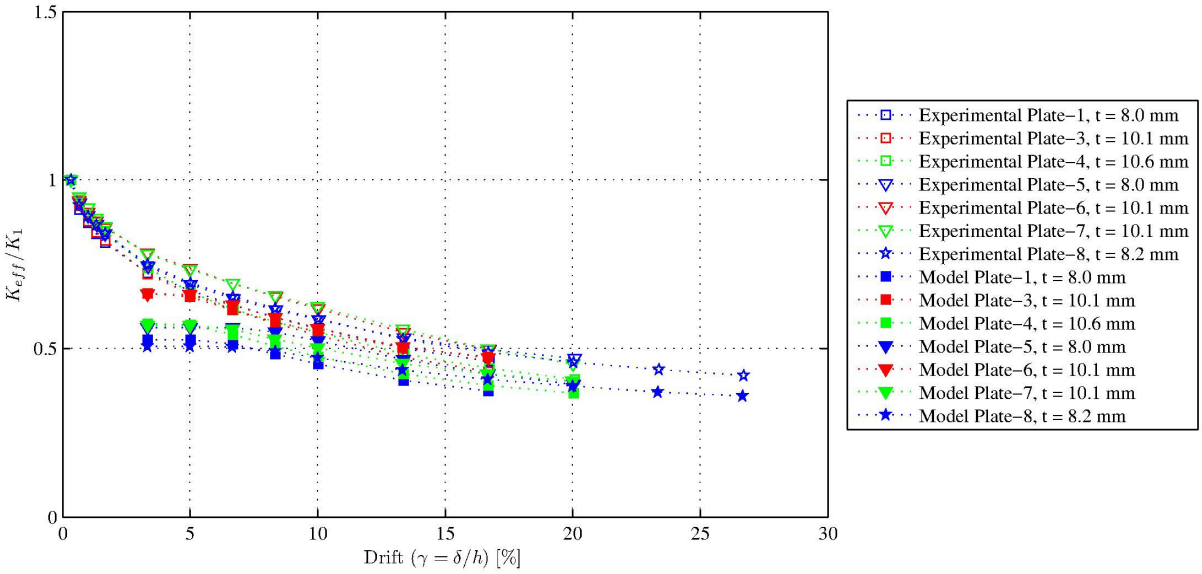

Figure 2.6. Normalized effective stiffness as a function of drift.

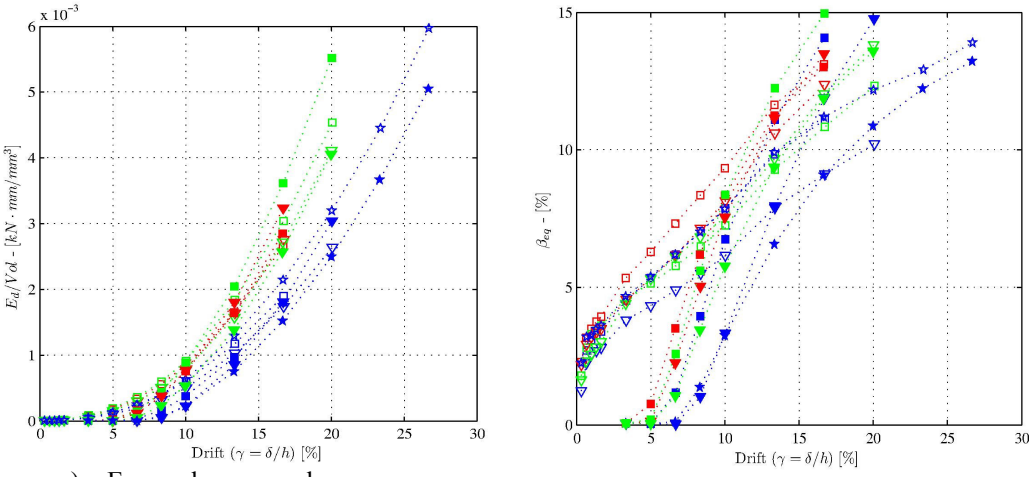

a) Energy loss per volume.

b) Equivalent damping ratio.

Figure 2.7. Energy loss and Equivalent damping ratio as a function of drift.

3. NUMERICAL STUDY

3.1. Constitutive law model

Using the experimental data from tensile coupon tests, the multilinear model proposed by Motahari and Ghassemieh (2007) (see Fig. 3.1), was calibrated applying a least square fit to the measured stress (σ_e) and the predicted stresses (σ_m), using the model parameters σ_s^{cr}, σ_f^{cr} , ε_L , and E_m as variables (see Eqn. 3.1).

$$\min_{\sigma_s^{cr},\sigma_s^{cr},E_m,\varepsilon_L} \int (\sigma_e - \sigma_m)^2 \, d\varepsilon \tag{3.1}$$

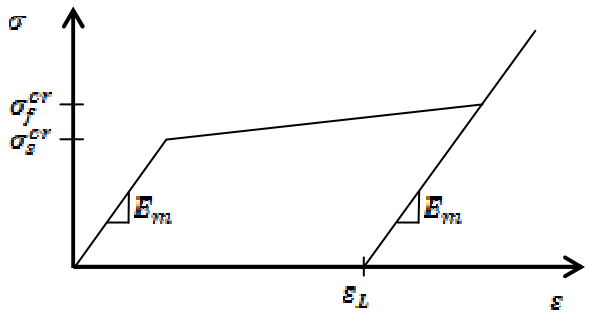

Figure 3.1. Model proposed by Motahari and Ghassemieh (2007).

Since the process of detwinning was not completed during the tests, there is more than one combination of σ_f^{cr} and ε_L which produces the same results, so an arbitrary value of ε_L = 3% was set for each test. It was found that a variation within acceptable ranges (3% - 6%) for this parameter does not affect the minimization results. The resulting parameter values are shown in Table 2. These yielding values agree with those determined directly from the tests curves (Fig. 2.3). Fig. 3.2 compares the experimental and analytical results of the calibrated material model. The analytical model presents an adequate correlation with the experimental results, although slightly over predicting the maximum stress at each cycle. One of the limitations of the model is that the critical transformation stress σ_s^{cr} is constant and independent of the strain.

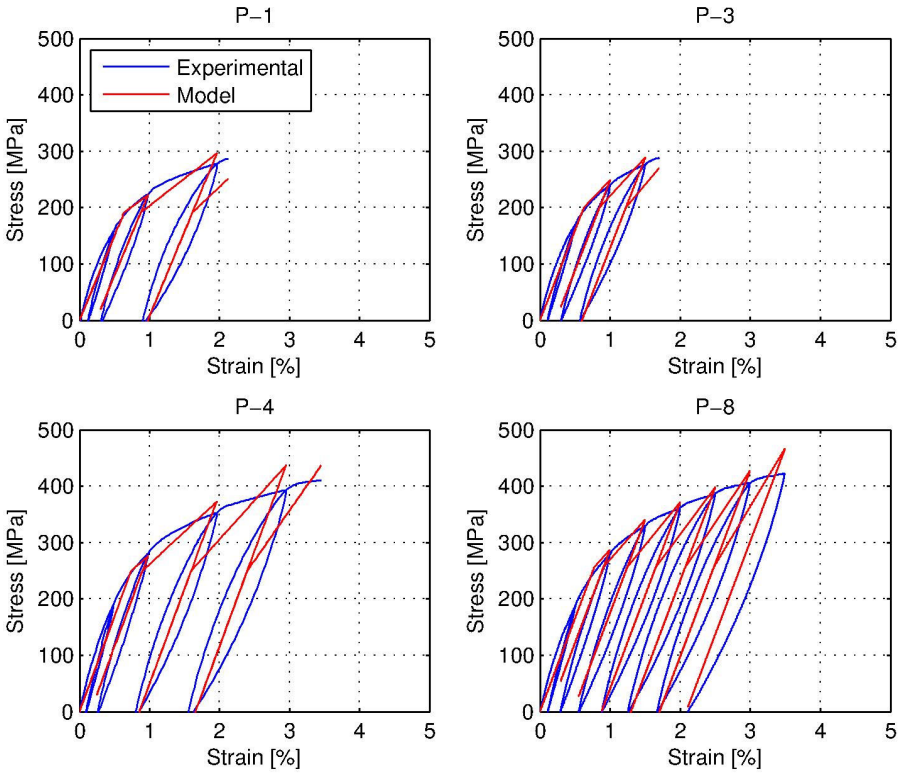

Figure 3.2. Comparison between experimental and analytical constitutive law.

Table 2. Model parameters from minimization process.

Coupon	E_m [GPa]	σ_s^{cr} [MPa]	σ_f^{cr} [MPa]	Alloy
P-1	29.9	191.0	584.8	A
P-3	31.9	199.0	858.3	A
P-4	33.7	249.4	750.1	B
P-5	33.6	275.6	641.3	B
P-6	35.0	250.3	850.1	B
P-7	30.4	242.5	815.3	B
P-8	33.1	255.4	974.0	B

3.2. Plate model

A finite element model was developed to predict the flexure plate behavior using MATLAB software (2009). The plate was divided in 16 segments along the height. Each segment has a constant width (equal to the average width of the segment) and it is represented by 10 uniaxial fibers which behavior is modeled by the previous obtained constitutive law (see Fig. 3.3). Fig. 3.4 shows the experimental and analytical force-displacement curves obtained for Plate-8.

Equivalent normalized stiffness, Energy loss per volume and Equivalent damping ratio were computed for each cycle. These results are included in Fig. 2.6 and Fig. 2.7. The model can predict the Equivalent stiffness, Energy loss per volume and Equivalent damping ratio with a maximum difference of 18%, 28% and 32%, respectively.

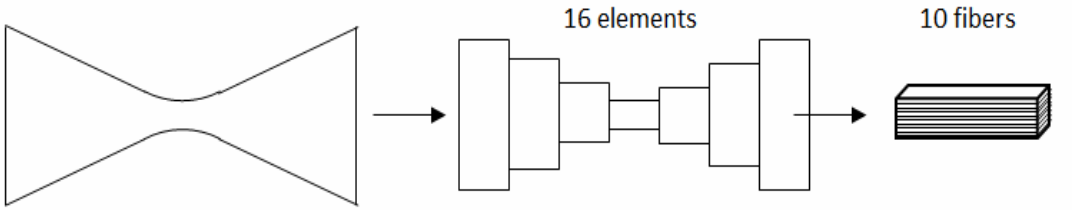

Figure 3.3. Schematic plate model

Theoretical expressions for the yielding point and elastic stiffness can be obtained from an elastic analysis of an idealized hour-glass shaped plate (Eqns. 3.2-3.4).

$$F_y = \frac{\sigma_y\, b\, t^2}{3\, h} \tag{3.2}$$

$$d_y = \frac{\varepsilon_y\, h^2}{2\, t} \tag{3.3}$$

$$K_{el} = \frac{F_y}{d_y} = \frac{2\, E\, b\, t^3}{3\, h^3} \tag{3.4}$$

Where σ_y and ε_y are the yielding stress and strain of the material. In this case, this point corresponds to the start of detwinning process on the martensite ($\sigma_y = \sigma_s^{cr}$ and $\varepsilon_y = \sigma_s^{cr} / E_m$). E is the Young Module of the material ($E = E_m$), b, h and t are the geometric properties of the hour-glass shaped plate (width at the ends, height and thickness respectively). In addition, a yielding point was computed on both the experimental and analytical curves by a bi-linearization of the envelope curve and the elastic stiffness and the yielding stress were compared with theoretical equations (Eqns. 3.2-3.4). The results are shown on Fig. 3.5a and 3.5b. The theoretical expressions and the finite element model give lower values for stiffness and yielding force (maximum difference of 33% and 42% for model and

theoretical stiffness and 26% and 40% for model and theoretical yielding force, respectively). This is due to the limitations of the constitutive material law, which underestimates the stiffness for low strains.

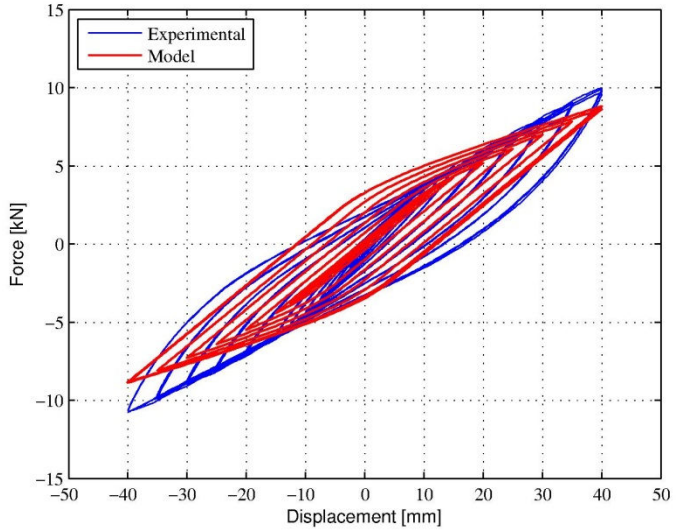

Figure 3.4. Comparison between experimental and analytical force-displacement curves.

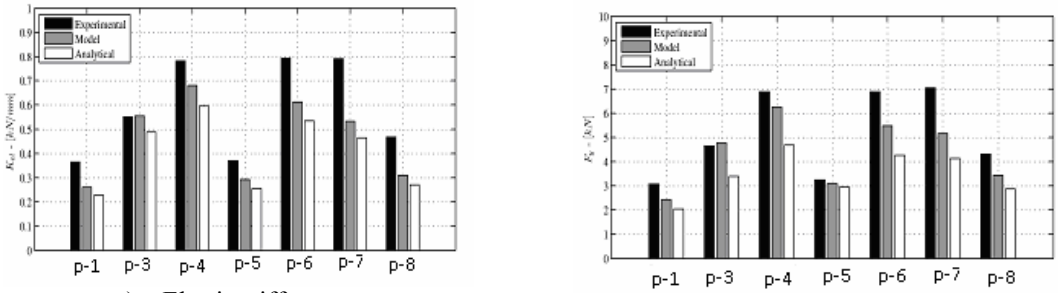

a) Elastic stiffness.

b) Yielding force

Figure 3.5. Elastic stiffness and Yielding force of each specimen.

4. CONCLUSIONS

Hour-glass shaped plates were fabricated using two CuZnAl alloys and tested under cyclic transverse flexure to study their potential as a seismic energy dissipation device. In addition, cyclic tension tests on material coupons were conducted to capture the material's constitutive law. A numerical study was conducted to predict the behaviour of the plates. The following major conclusions can be drawn:

- Alloy A has slightly less ductility than alloy B and both are in martensite phase at room temperature.
- No dependency on the excitation frequency (between 0.025 and 1 [Hz]) was observed.
- Plates dissipate energy through repeated stable hysteresis cycles without strength degradation. The behaviour is nonlinear and depends on the displacement amplitude: With increasing amplitudes, effective stiffness decreases and tends to stabilize at around 40-50% of the original value, and energy loss and equivalent damping ratio increases. Equivalent damping ratio reaches values of up to 13%.
- The model used for the constitutive law of the material adequately captures the experimental strain-stress behaviour, even though the detwinning process was not completed.

- The proposed nonlinear plate model can be used to predict the plate global behaviour and properties (effective stiffness, energy loss and equivalent damping ratio), for drift over 10%. On the contrary, a comparison between theoretical expressions (for an idealized hour-glass shape), experimental results and analytical results for the yielding point and elastic stiffness shows difference larger than 20%-30%.

AKCNOWLEDGEMENT

The authors gratefully acknowledge the financial support of CONICYT, Chile, through FONDECYT project 11090196. The first author acknowledges the financial support from CONICYT Fellowships for Graduate Studies Program. The work conducted at Georgia Institute of Technology was possible thanks to the funding provided by the Program for Short Research Stays of the Department of Graduate Studies, University of Chile, and the important contribution of Professor Reginald DesRoches and Postdoctoral fellow Chuang-Sheng Yang at Georgia Institute of Technology.

REFERENCES

Asgarian, B. and Moradi, S. (2011). Seismic response of steel braced frames with shape memory alloy braces. *Journal of Constructional Steel Research,* **67:1**,65-74.

Casciati F., Van der Eijk C., (2008). Variability in mechanical properties and microstructure characterization of CuAlBe shape memory alloys for vibration mitigation. *Smart Structures and Systems,* **4:2,** 103-121

Dong, J., Cai, C.S. and Okeil, A.M. (2011). Overview of potential and existing applications of shape memory alloys in bridges. *Journal of Bridge Engineering,* **16:2**,305-315.

Gibson, P. (2008). Fabricación y caracterización de una aleación con memoria de forma CuZnAl considerada para disipadores sísmicos. Mechanical Engineering Thesis, Universidad de Chile, Chile.

Johnson, R., Padgett, J.E., Maragakis, M.E., DesRoches R., Saiidi, M.S. (2008). Large scale testing of nitinol shape memory alloy devices for retrofitting of bridges. *Smart Materials and Structures,* 17:3.

MATLAB. Version 7.8.0.347 (R2009a) February, 2009, www.mathworks.com

Montecinos S., Cuniberti A., and Sepúlveda A. (2008). Grain size and pseudoelastic behavior of a Cu-Al-Be alloy. *Materials Characterization,* **59:2,** 117-123.

Motahari, S.A. and Ghassemieh, M. (2007). Multilinear one-dimensional shape memory material model for usein structural engineering applications. *Engineering structures,* **29:6**,904-913.

Speicher M.S., DesRoches R., and Leon R.T., (2010). Behavior of a SMA-partially restrained beam-column connection. *9th US National and 10th Canadian Conference on Earthquake Engineering.* Paper Nº982

Vargas, J. (2007). Ensayo de placas tipo ADAS de láminas de CuZnAl. Civil Engineering Thesis, Universidad de Chile, Chile.

Youssef, M.A., Alam M.S. and Nehdi M. (2007). Experimental Investigation on the Seismic Behavior of Beam-Column Joints Reinforced with Superelastic Shape Memory Alloys. *Earthquake Engineering.* **11:2,** 1205-1222.